Journal of *Marine Science and Engineering*

MDPI

Article

Effects of Biological Adhesion on the Hydrodynamic Characteristics of Different Panel Net Materials: A BP Neural Network Approach

Yongli Liu [1], Wei Liu [1,†], Lei Wang [1,*], Minghua Min [1], Lei Li [1], Liang Wang [2] and Shuo Ma [1]

[1] East China Sea Fisheries Research Institute, Chinese Academy of Fishery Sciences, Shanghai 200090, China; 15921847103@163.com (Y.L.); 18817771740@163.com (W.L.); minmh@eastfishery.ac.cn (M.M.); zheyilee@126.com (L.L.); mas@ecsf.ac.cn (S.M.)

[2] Mineral Resources Development Center, Zhucheng Natural Resources and Planning Bureau, Weifang 262200, China; 18616830063@163.com

* Correspondence: emperor0228@163.com; Tel.: +86-216-566-8440; Fax: +86-216-568-3926

† Co-first author.

Abstract: Biofouling is a serious problem in marine aquaculture facilities, exerting several negative effects on cage structures. In this study, different materials of nets were placed in the Fujian Sea area of China, and the main biological adhesion species were determined. The drag force of different materials of fouled nets was studied by a physical test in a flume tank. The drag force coefficient of a clean polyethylene terephthalate (PET) net was 0.53. The drag force coefficients of ultrahigh-molecular-weight polyethylene (UHMWPE) and polyethylene (PE) nets were 161.2% and 133.5% higher, respectively, compared with those of PET nets. Crustaceans, mollusks, and algae were the main organisms that adhered to the nets. Compared with the clean nets, the drag force of PET, UHMWPE, and PE nets increased by 1.29–5.06 times, 1.11–2.85 times, and 0.55–2.46 times, respectively. Based on backpropagation (BP) neural network training, the relationship between biological characteristics (average adhesion thickness and density) and the drag force of three kinds of net materials was determined. The drag force of the biofouled net at various time points throughout the year can be predicted based on this model, which can guide the cleaning and maintenance of nets in cage structures.

Keywords: panel net; biological adhesion; hydrodynamic characteristics; density

Citation: Liu, Y.; Liu, W.; Wang, L.; Min, M.; Li, L.; Wang, L.; Ma, S. Effects of Biological Adhesion on the Hydrodynamic Characteristics of Different Panel Net Materials: A BP Neural Network Approach. *J. Mar. Sci. Eng.* **2024**, *12*, 2064. https://doi.org/10.3390/jmse12112064

Received: 10 October 2024
Revised: 7 November 2024
Accepted: 12 November 2024
Published: 14 November 2024

1. Introduction

Aquaculture is among the fastest-growing areas of food production worldwide, contributing significantly to global food security and high-quality protein supplies; marine cage farming constitutes an important part of aquaculture [1]. As a core component of the marine cage culture system, a suitable net is crucial for marine culture production. Conventional polyethylene and nylon nets are susceptible to fouling organisms [2]. The adhesion of marine organisms to cage nets has emerged as a global problem, increasingly affecting the mariculture industry [3]. It reduces the volume of the cage, shrinks the mesh, increases the drag force of the cage anchor system [3], and seriously increases the weight of the cage, further causing the cage to sink and net deformation [2,3]. Biological adhesion can cause direct physical damage to the net and accelerate its aging. Shrinking mesh size can reduce the flow velocity, exchange of nutrients, and diffusion and dilution of the excrement of the farmed organisms [4]. Simultaneously, the dissolved oxygen content is disturbed, especially in summer when the amount of fouling biological attachment is large. The fouling biological attachment and higher water temperature, coupled with the respiration activities of the fouling organism itself, can further aggravate the decline in dissolved oxygen content, and anoxia may occur in severe cases. This affects aquaculture

production and the surrounding marine environment, resulting in local eutrophication and other negative effects [5]. The biological adhesion can provide a place for parasites and pathogenic microorganisms to live, potentially harming the health of farmed organisms [6]. Physical and chemical methods, such as net change, manual or machine cleaning, anti-fouling coating, and input of chemical products, are commonly employed in marine cage aquaculture practices to remove fouling organisms; however, these methods can also adversely affect the surrounding marine environment and are ineffective in some cases [7]. This increases the breeding costs and reduces income [8]. Therefore, studying the hydrodynamic characteristics of biologically fouled nets for designing and maintaining cages is crucial.

In the past few decades, many scholars [9–12] have conducted several experiments using physical models and numerical simulations on the hydrodynamic characteristics of nets and cages and obtained many hydrodynamic coefficient values and mechanical characteristics of clean nets. However, there are few published studies on the hydrodynamic characteristics of cages or nets with fouling organisms attached. Lader et al. [10] used the mesh data obtained from field tests in a farm in Norway as reference data for net ropes attached to an artificial hydroid and measured the force of net ropes through laboratory flume experiments. As a result, the fitting curve of the drag force coefficient was as follows: for the twine with the shortest hydroids (9 mm), the drag was from 1.5 times (Re = 4000) to 2.2 times (Re = 1000) the drag on clean twine; for the longest hydroids (21 mm), the drag was 2 times and 3.8 times that on clean twine, respectively. Farshad et al. [11] generated a full-size gravity cage model. The net comprised polyester (PES) material, and the simulated fouling organisms were wound on the mesh with nylon rope of different lengths to obtain cages of different densities. Bi et al. [12] established a porous media model to simulate the biologically attached mesh, and studied the characteristics of the prototype scale, including the internal and external fields of the cage under water flow. Compared with the clean cage, the flow velocity decreased as the biological adhesion increased, and the flow field distribution became disordered inside the cage gradually. On this basis, Bi and Xu [13] simulated the flow field characteristics of a cage array (taking a 2×4 cage array as an example) under a tidal current. In general, the greater the degree of biological attachment, the more obvious the influence on the tidal current field around the cage. Compared with the results without considering the effect of biological attachment, the presence of attachments changed wave fields inside and outside the cage significantly. After a wave propagates through the cage array, its crest and trough are reduced due to the damping effect of the cage and the attachment [14]. Swift et al. [15] studied the stress characteristics of the attached panel net of marine organisms and measured the stress of the net with different adhesion degrees under the current by laboratory model tests and field measurements. Lader et al. [10] used model tests to analyze the stress characteristics of net-attached organisms in water flow. The results showed that the stress of the net was closely related to the length, growth time, and Reynolds number of the attached organism. Gansel et al. [16] used a physical model test to analyze the hydrodynamic characteristics of the panel net under water flow by an attachment such as a hydroid, and obtained the relationship between the drag force on the net and the density of the biological adhesion. Bi et al. [17] conducted a field hanging test and obtained a mesh with different biological attachment degrees by controlling its depth and duration of immersion. A series of physical model tests were conducted in a flume tank to measure the drag force and corresponding drag force coefficient of mesh with different adhesion degrees at different flow velocities. The attachment can increase the drag force on the net by more than 10 times. Different twine preparation (degree of twist, multifilament, monofilament, etc.) processes change the surface structure and texture of the twine, thus affecting the biological attachment. Dos Santos et al. [18] suggest that compared with monofilament twine, the surface of multifilament twine is rougher, which makes it easy for marine organisms to attach and increases the mesh's hydrodynamic force. Therefore, in the actual

breeding process, attention should be paid to the timely cleaning or replacement of mesh clothing [19].

Although much progress has been made, the effects of biological pollution on the hydrodynamic characteristics of fishing nets have not been systematically studied, necessitating studies on the hydrodynamic properties of the net under different biological pollution levels. The variety of organisms attached to the net varies, depending on the sea area and the season. Physical and geometric characteristics and the distribution of different types of biological fouling exert different effects on the hydrodynamic characteristics of the cage. Quantifying the effects of biological pollution with various physical and geometric characteristics on the hydrodynamics of aquaculture nets is necessary. To this end, the present study first (i) classified and statistically analyzed the main adhesion organisms of three kinds of panel net material, namely PET, UHMWPE, and PE, in different months in the East China Sea and (ii) explored the effects of biological adhesion characteristics (thickness and density) on the drag force performance of each net through a dynamic flume test. Finally, (iii) the BP neural network was trained to fit the relationship between the biological adhesion characteristics and the drag force performance of the net. The findings can provide a scientific basis for the application screening of new materials, maintenance, and cleaning strategies for the net in the marine cage culture.

2. Materials and Methods

2.1. Area and Time of Sea Trials

The experimental operation was conducted from October 2021 to September 2022, within the East Sea near Fujian Province (25.24° N, 119.54° E) (Figure 1). The operating sea depth was 15–20 m.

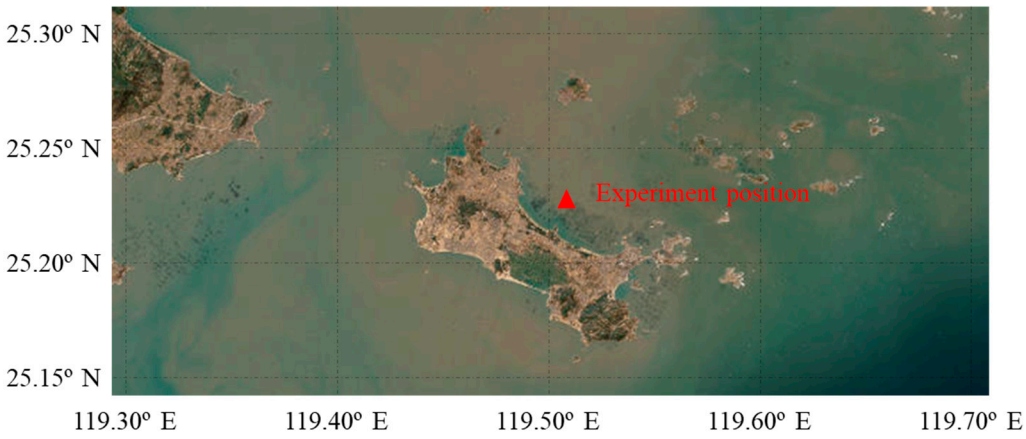

Figure 1. Geographic maps showing the experiment position.

2.2. Experimental Net

The experimental net materials selected were determined according to the net used on the aquaculture cage, including PET, UHMWPE, and PE. The size of the breeding object, a large yellow croaker (*Larimichthys crocea*), was 0.5–0.6 kg, requiring the selection of net material with a twine diameter of 3.0 mm and a mesh size of 50–70 mm. The mesh shape of PET and UHMWPE was hexagonal, and that of PE mesh was diamond. The parameters of the experimental nets are shown in Figure 2.

2.3. Experimental Equipment and Procedures

The mesh material was fixed with a steel bar frame matching its size, which was rectangular as a whole. Nylon cable ties were used to fix the mesh material on the steel bar frame, and the spacing of the mesh material was fixed to maintain its randomness. PE twine was used to connect the mesh material in series at the outer four corners. The net pieces of three different net materials were hung in the sea area where the fan was installed in Fujian.

The water depth for the hanging was 5.0 m, and the size of the net pieces was 0.3 m × 0.3 m. During the experiment, the net pieces at sea were tied with cable ties on a square frame of 0.3 m × 0.3 m with a diameter of 6.0 mm for testing (Figure 3). The hanging time of the mesh was 1 year, and sampling was performed on the 25th of each month. During sampling, the ship's windlass was used to pull the rope out of the sea to sample. The net group was disassembled and divided into individual net garments, packed flat in PE-sealed bags, and brought back to the laboratory for analysis of the classification number.

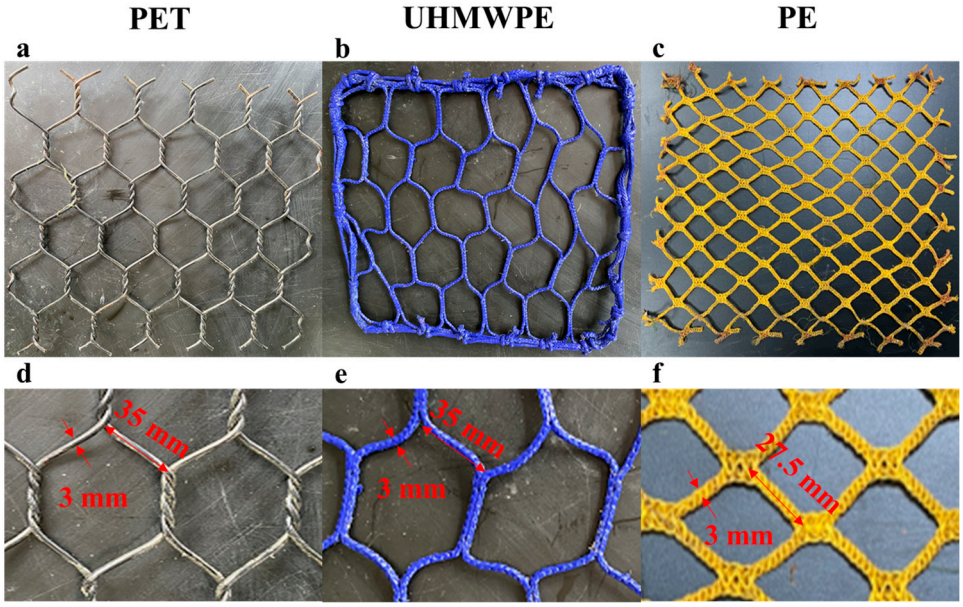

Figure 2. Overview of the different material experimental nets (**a**–**c**) and the nets in detail (**d**–**f**).

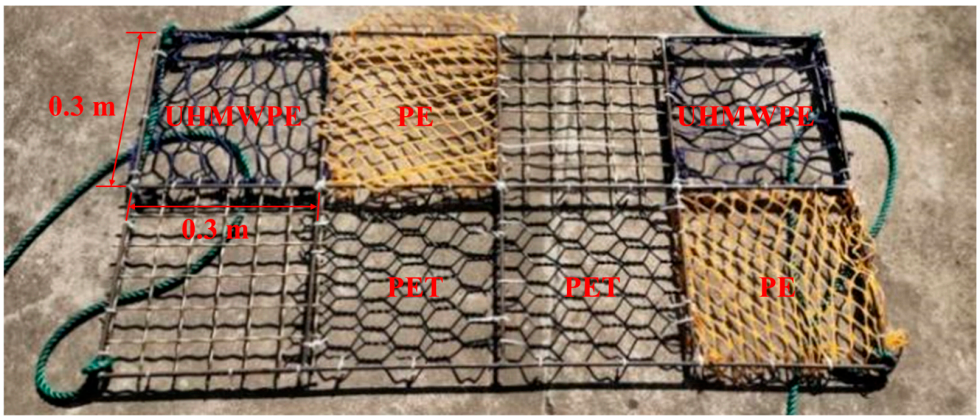

Figure 3. Schematic diagram showing the fixing of the nets.

The experiment was conducted in the circulating flume tank at the East China Sea Fisheries Research Institute (Figure 4). The circulation flume tank measured 1.8 m (length) × 0.5 m (width) × 0.5 m (depth) and contained ~450.0 kg of freshwater (density: 998.2 kg/m^3; temperature: 17.6~18.4 °C). The maximum flow rate was 2.5 m/s. A front view window of the tank allows the users to observe the behavior of the nets during testing. To reliably measure hydrodynamic forces, the panel net was attached to a rigid frame with a side length of 0.3 m and submerged in water to a depth of 0.1 m. A current meter was installed approximately 2.0 m upstream of the panel net to detect the flow velocity. Hydrodynamic force signals were measured using a six-component load cell with capacities of 5.0 kg each and a specified accuracy of 2.0%. These hydrodynamic force signals were amplified using a dynamic strain amplifier (DPM-6H), and then sent to an A/D converter and a computer. The data were sampled at 100 Hz.

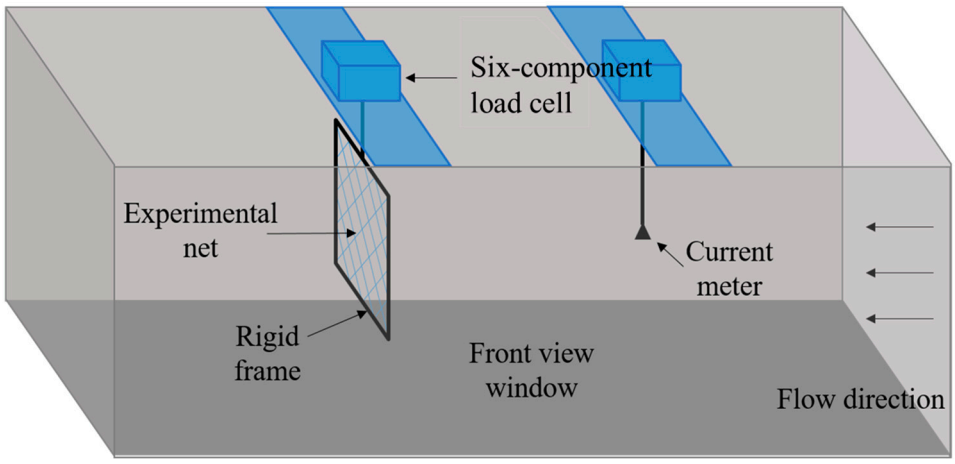

Figure 4. Schematic of flume tank and equipment.

The drag force of the net was determined by subtracting the frame drag from the drag of the combined structure (panel net and rigid frame). The rigid frame was connected to the six-component structure of the load cells, resulting in the plane of the rigid frame being perpendicular to the current direction. These load cells were calibrated and zeroed at each test's beginning and end, and linearity was confirmed. The drag force of the frame was measured at different flow velocities, ranging from 0.2 to 1.3 m/s with an interval of 0.1 m/s. The measurements of the combined structure were conducted at five different flow velocities (0.4 m/s, 0.6 m/s, 0.8 m/s, 1.0 m/s, and 1.2 m/s). The rigid frame and panel net were assembled into the six-component instrument, making the rigid frame plane perpendicular to the flow direction. Finally, the relationship between the drag coefficient and Reynolds number (800–4200) was established to evaluate the effects of biological adhesion to the net and the drag force.

2.4. Data Extraction

The identification and analysis of biological attachment nets mainly focused on (i) adhesion species composition, (ii) adhesion thickness, and (iii) adhesion density.

(i) The methods of identification of the attached species were as follows: observation and identification with a microscope, and reference to *Zoology of China*, the *Atlas of Marine Life of China*, and other books. Seasonal changes in the community were analyzed according to the results of identification.

(ii) The measurement method for adhesion thickness was as follows: five areas with attached organisms on the top, bottom, left, and right of the mesh material were selected to determine the thickness with a vernier caliper, and the average value was obtained.

(iii) The method of density calculation was as follows: input the image, adjust image size, select a valid region, calculate the valid region area (D1), perform image automatic threshold segmentation, calculate the attachment and net area (D2), and output the data measurement (D2/D1) × 100%. Among these steps, the selection process of the valid region was as follows: by positioning the vertex coordinates of the four sequential corners of the mesh, the enclosed quadrilateral was divided into two triangles. The point coordinates of the two triangles were entered into the program to calculate the area using Helen's formula, and the areas of the two triangles were added to obtain the area of the quadrilateral (Figure 5a–c). The effect diagram of automatic threshold segmentation is shown in Figure 5d–f.

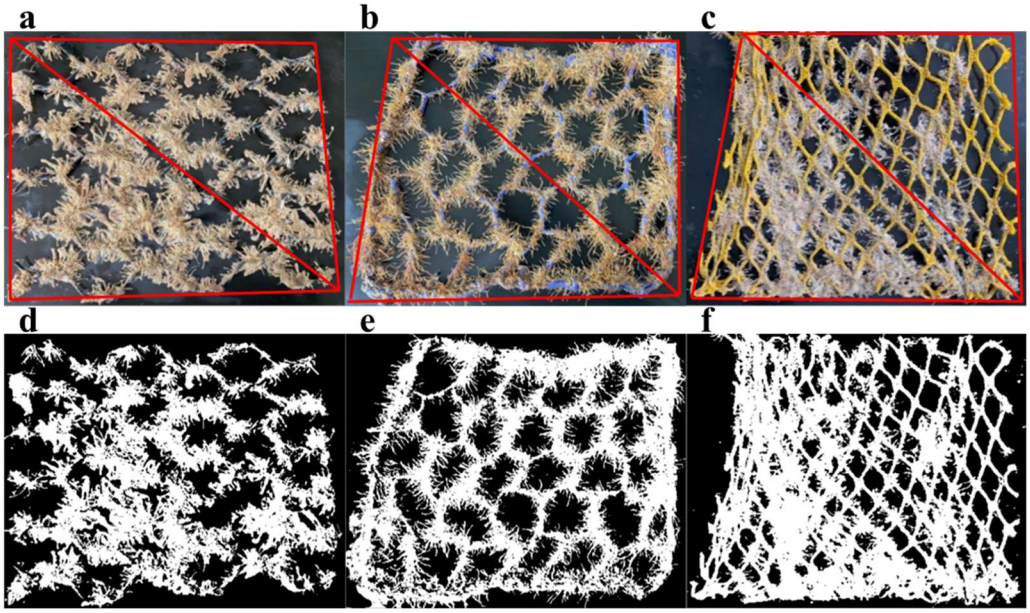

Figure 5. The quadrilateral was selected and divided into two triangles (**a**–**c**), and the automatic threshold segmentation effect is shown (**d**–**f**).

2.5. Data Analysis

The drag coefficient was calculated using Equation (1) as follows:

$$C_x = \frac{2R}{\rho S V^2} \text{ or } C_{rx} = \frac{2R}{\rho S_a V^2} \quad (1)$$

where C_x is the drag coefficient, C_{rx} is the relative drag coefficient, R is the drag force, ρ is the density of water (=998.2 kg/m^3), S is the net twine areas, S_a is the average biological adhesion density, and V is the flow velocity.

The Reynolds number represents the ratio of inertial and viscous forces and is calculated as follows:

$$Re = \frac{Vd}{v} \text{ or } Re = \frac{Vd_a}{v} \quad (2)$$

where Re is the Reynolds number, d is the twine diameter, da is the average biological adhesion thickness, and v is the kinematic viscosity (=0.001005 Pa*s).

Backpropagation is an algorithm used to train a neural network in machine learning [20]. Figure 6 shows the structure of the BP neural network. X_i represents the experimental values, which are input values for the input layer (i = 1, 2, . . ., n), and n is the number of the input layer; w_{ij} is the weight of the j-th hidden layer from the i-th input layer (j = 1, 2, . . ., p), and p is the number of the hidden layer; w_{jk} is the weight of the k-th output layer from the j-th hidden layer (k = 1, 2, . . ., m), m is the number of the output layer, and Y_k is described as the objective value. For transfer functions from the input to the hidden layer and from the hidden to the output layer, a tangent sigmoid transfer function (tansig) and a linear transfer function (purelin) are chosen and denoted as follows, respectively:

$$H_j = f\left(\sum_{i=1}^{n} w_{ij} X_i - a_j\right) \quad (3)$$

$$f(x) = \frac{1}{1 + \exp(-1)} \quad (4)$$

$$O_k = \sum_{j=1}^{p} \left(w_{jk} H_j - b_k\right) \quad (5)$$

where a_j and b_k are threshold values for the hidden and output layers. O_k is the predicted value. The error (e_k) different from the expected value Y_k is demonstrated as follows:

$$e_k = Y_k - O_k \tag{6}$$

In each iteration, the weight and threshold values were trained by referring to the gradient descent backpropagation as follows:

$$w_{ij} = w_{ij} + \eta H_j(1 - H_j) X_i \sum_{k=1}^{m} w_{jk} e_k \tag{7}$$

$$w_{jk} = w_{jk} + \eta H_j e_k \tag{8}$$

$$a_j = a_j + \eta H_j(1 - H_j) \sum_{k=1}^{m} w_{jk} e_k \tag{9}$$

$$b_k = b_k + e_k \tag{10}$$

where η is the learning rate coefficient (η = 0.1 in this study). The root mean square error (RMSE) less than the order of negative four was applied for convergence. The number of hidden layers was determined using the regression R^2-value. In this study, the flow velocity, average thickness, and average density were the experimental values of the four input layers, and drag force was the objective value of the output layers. The number of units for the hidden layer was chosen as 16 since the excellent prediction accuracy with the regression R^2-value was close to 1 in our pretest work. The procedure was conducted using Matlab (The MathWorks Inc., Portola Valley, CA, USA).

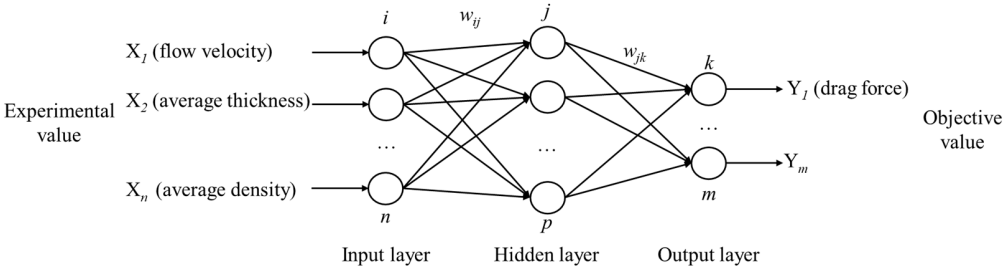

Figure 6. Topology diagram of the BP neural network in the present study.

3. Results and Discussion

3.1. Drag Force on Nets Without Biological Adhesion

The drag force on the nets was determined by subtracting the average measurements for each flow velocity on the rigid frame from the average measurements for each flow velocity on the frame and nets. The results are shown in Figure 7. The drag force on different nets increased as the flow velocity and attack angle increased. The drag forces on the PE net were 239.95 ± 5.80% and 54.91 ± 5.58% greater than those on the PET and UHMWPE nets, respectively.

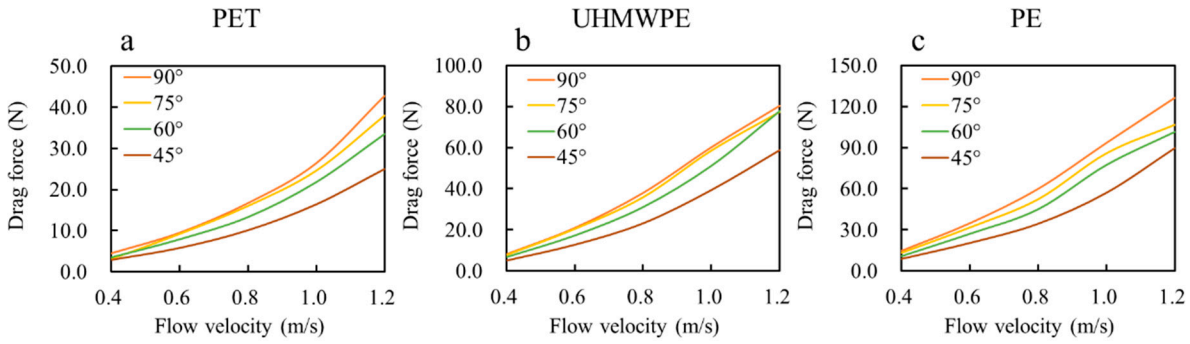

Figure 7. Drag force on different nets at four attack angles and five flow velocities.

On average, the drag force coefficients were 0.52 ± 0.03, 1.37 ± 0.08, and 1.23 ± 0.04 of the PET, UHMWPE, and PE nets at a 90° attack angle, respectively (Figure 8). The drag force coefficients of the nets were increased with the increase in the attack angle but did not change with an increased Reynolds number. Moreover, the twine area of the PE net was the largest (15,120 mm^2); specifically, it was 45.45% and 82.28% larger than those of the PET and UHMWPE nets. The results showed that the PET net had the smallest drag force for the same twine area, which may be mainly related to the twine structure. The PET net uses monofilament twine, while UHMWPE and PE comprise braided twine, leading to a relatively small surface smooth drag for PET. The drag force coefficient of the UHMWPE net was larger than that of the PE net, which may be caused by the different weaving modes of the twines. The shape of the UHMWPE twine was cylindrical, while that of the PE mesh was flat with better filterability. When the water flowed through the twines, the cylindrical UHMWPE net showed relatively poor filterability due to the structure of the twine, resulting in a greater drag force coefficient.

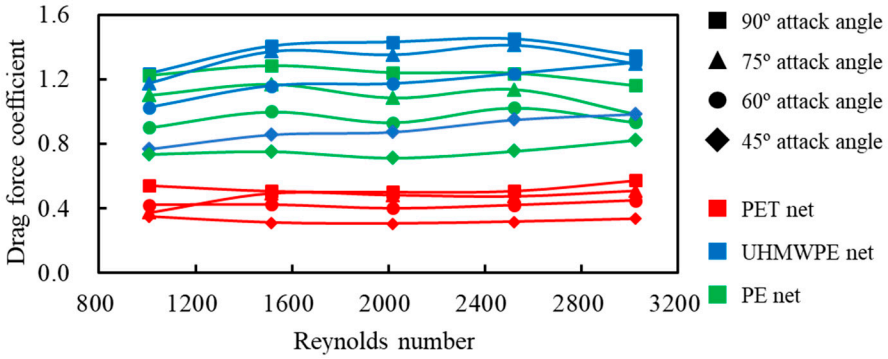

Figure 8. Drag force coefficients for different nets at different Reynolds numbers.

3.2. Biological Adhesion Characteristics of Different Nets in Different Months

In spring, 24 species adhered on the experimental nets, including 9 species of crustaceans, 5 mollusks, 5 algae, 3 annelids, 1 cnidarian, and 1 bryophyte, which accounted for 37.50%, 20.83%, 20.83%, 12.50%, 4.17%, and 4.17%, respectively (Figure 9A–I). The number of species adhered on the experimental nets in summer was the largest (43 species), with crustaceans and mollusks accounting for 13 species (30.23%), and 7 more algae species (16.28%) compared with spring, along with 4 annelids (9.30%), 3 cnidarians (6.98%), 2 moss animals (4.65%), and 1 echinoderm (2.33%) (Figure 9J–R). In autumn, 35 species of adhered organisms were identified on the three nets of different materials. The number of crustaceans was the largest, with 14 species, accounting for 40.00% of the total species, 6 species of mollusks, accounting for 17.14%, 5 kinds of algae, accounting for 14.29%, and 4 annelids (11.43%). Moreover, there were two cnidarians and two echinoderms, accounting for 5.71%, and one bryophyte (2.86%) and one chelicera (2.86%) (Figure 9S–a). In winter, the number of species of adhered organisms on the experimental nets was the lowest (21 species). The number of crustacean species was the highest (seven species, accounting for 33.33% of the total species). There were five species of mollusks and algae, accounting for 23.81%; three annelids accounted for 14.29%, and one cnidarian accounted for 4.76% (Figure 9b–j).

The classification and statistical analysis showed that the organisms attached to the net in the East China Sea were mainly crustaceans, mollusks, and algae. In Norway, cages are associated with a wide variety of biological fouling organisms, such as hydroids, mussels, and algae [21]. In Norway, which is the leading producer of Atlantic salmon, the hydroid (*Ectopleura larynx*) dominates biofouling communities on coastal fish farms during the peak of the biofouling season [22]. Therefore, the biofouling of hydroids on salmon cage nets poses an urgent concern for the Norwegian finfish industry. Bi et al. [17] found that the attached organisms in the Yellow Sea of China include hydroids. The difference between the results of this study and those of others is mainly due to different marine environments.

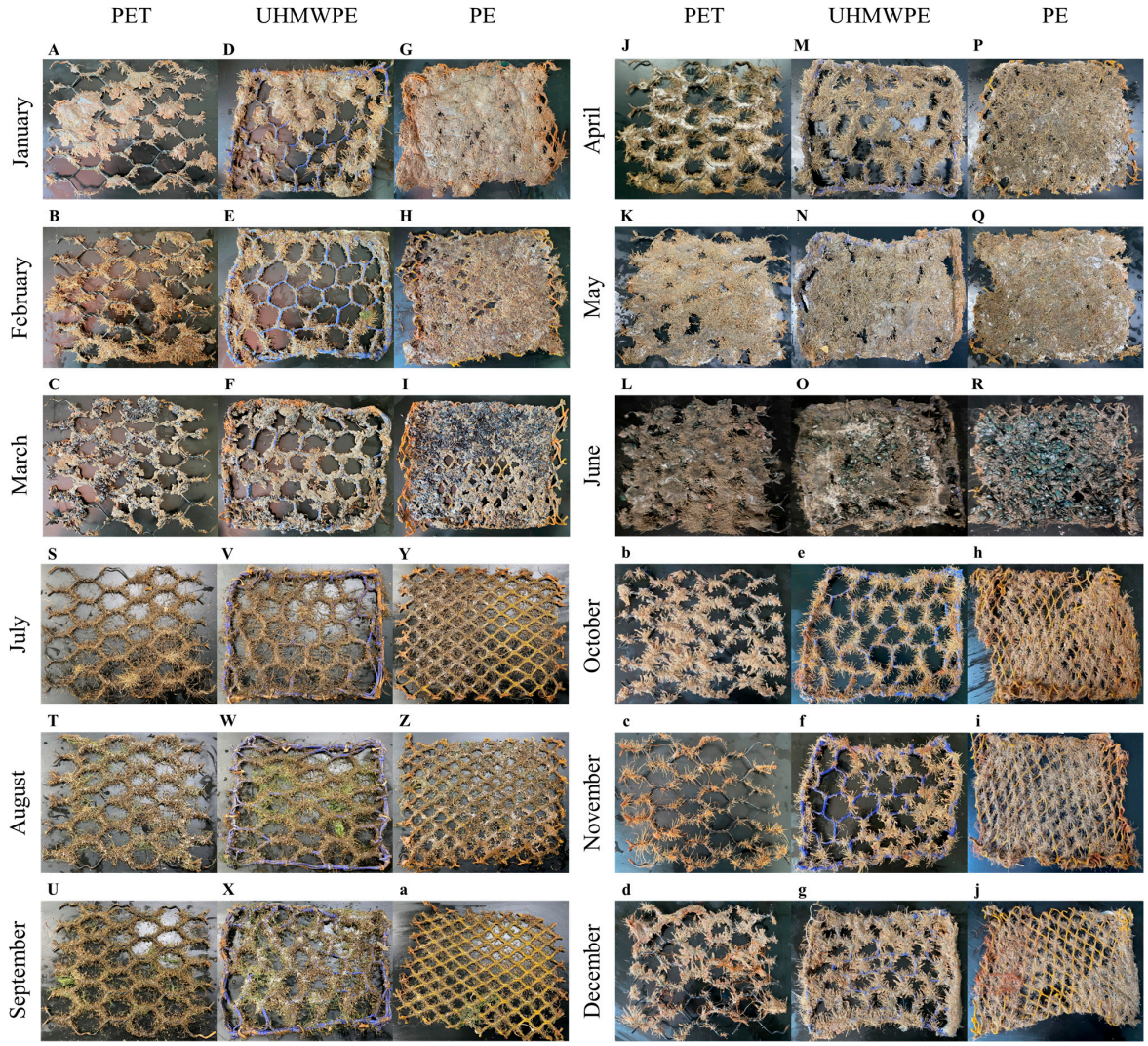

Figure 9. Biological adhesion on three nets of different materials in different months ((**A**–**I**): in spring; (**J**–**R**): in summer; (**S**–**a**): in autumn; (**b**–**j**): in winter).

The biological adhesion thickness of the three material nets was the largest in January and began to decrease thereon, showing fluctuations from March to December. The thickness of biological adhesion on the PET net was maintained at 12.40 ± 2.16 mm–19.30 ± 0.50 mm. The biological adhesion thicknesses of UHMWPE and PE nets ranged from 13.90 ± 1.62 mm to 21.00 ± 1.00 mm and 14.00 ± 5.00 mm to 22.30 ± 0.40 mm, respectively (Figure 10a). The densities of biological adhesion of the PET and UHMWPE nets were maintained at 44.32 ± 3.96% and 50.93 ± 7.07%. The densities of the PET and UHMWPE nets showed little change in the first three months, and from March to May, the biological adhesion on the two material nets increased significantly, reaching the maximum in May. Subsequently, it decreased. From October to December, biological adhesion on the PET net was maintained at 34.15 ± 2.99%, while the biological adhesion on the UHMWPE net increased. The biological adhesion on the PE net reached 96.20 ± 2.47% in January and subsequently began to decrease, dropping to 65.91 ± 9.04% in March. From April to June, the density of biological adhesion on the mesh began to increase, reaching the maximum in June, and then decreased. Similarly, the density of biological adhesion was low in October and remained at 52.74 ± 3.30%. In summary, the biological adhesion thickness and density of the PE net were larger than those of the PET and UHMWPE nets. The PET net showed the lowest biological adhesion thickness and density (Figure 10b).

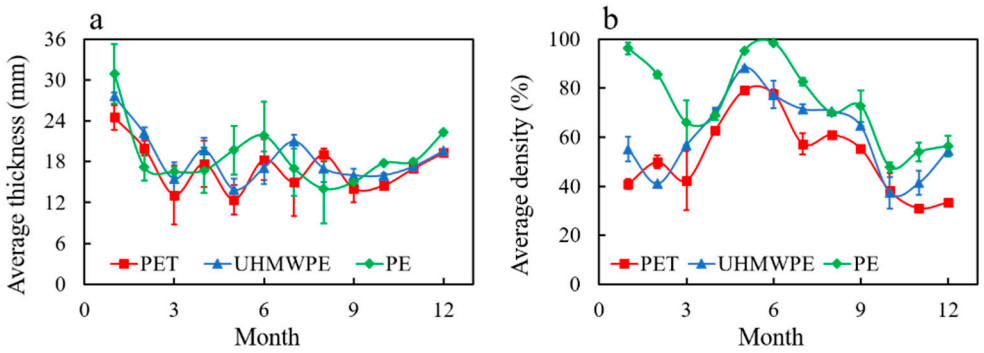

Figure 10. Average biological adhesion thickness (**a**) and density (**b**) of nets of three materials in different months.

The nets of PE and UHMWPE were braided, with many gaps in the twine, thus providing conducive attachment conditions for marine organisms. The net of PE was diamond-shaped, and the solidity ratio was smaller than that of UHMWPE, so the tentacles of marine-attached organisms were more easily attached to the net twine. Bi et al. [17] studied the effects of biological attachment to the net on the hydrodynamics of the net in the fishing ground of the Yellow Sea in China. The attached organisms on the net were mainly hydroids in autumn. The biological pollution level of the panel net was significantly positively correlated with the inundation time. However, in this study, the attached organisms on the net in the Fujian Sea of China were mainly crustaceans, and the biological pollution level of the panel net was correlated with the season. Biological pollution was not more serious with longer submersion times. The biological pollution level and the inundation time in autumn were negatively correlated. The reason may be that the dominant organisms in different sea areas are different, and the growth cycles of organisms also differ. This results in a gradual increase in hydroids attached to the Yellow Sea in autumn, while the number of crustaceans in the Fujian Sea gradually decreases.

3.3. Hydrodynamic Characteristics of Biological Adhesion Nets in Different Months

The drag force of the biological adhesion nets of the three materials is shown in Figure 11. The drag force of the three material nets was increased with an increase in flow velocity. The drag force of the PET net was smaller than that of the UHMWPE and PE nets, while the drag force of the PE net was the highest under the same conditions. Specifically, in January, at 1.2 m/s, the drag force of the PET net was 74.1 N and increased, then decreased. The drag force began to increase in April until the drag force was largest in July. By August, the drag force of the PET net plummeted to 47.2 N, and the change was stable. In December, the drag force was 43.2 N (Figure 11a). The drag force of the UHMWPE and PE nets decreased first and increased in spring. The drag force of UHMWPE and PE nets gradually decreased from April to August. Finally, it began to increase in August, reached the maximum in October, and then began to decrease until December (Figure 11b,c).

In fluid dynamics, the drag coefficient is a dimensionless quantity used to quantify an object's drag or resistance in a fluid environment. Usually, the area used in drag calculations is the projection area [10,14,23]; for nets, however, the outline area is also used [15,16,24]. The drag coefficient based on the projection area of a panel net is primarily related to the drag behavior of the net strand or the biofouling, while the drag coefficient based on the outline area is directly related to the drag force acting on a panel net.

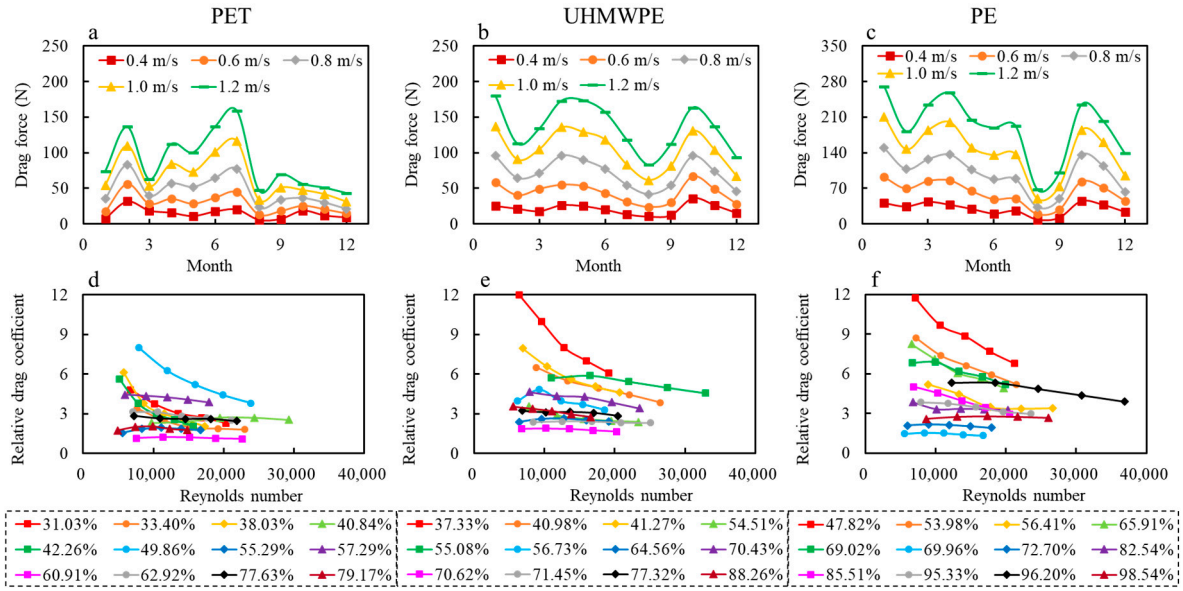

Figure 11. Drag force (**a**–**c**) and relative drag coefficients (**d**–**f**) of nets of three materials in different months and at different average biological adhesion densities.

With the increase in the Reynolds number, the drag force coefficient of the biological adhesion mesh was unchanged after decreasing. In contrast, the drag coefficient had no obvious relationship with the biological adhesion characteristics of the mesh. It showed a tendency to decrease first and then increase slightly with an increase in the density of biological adhesion. Specifically, at the same Reynolds number, when the densities of biological adhesion on the PET, UHMWPE, and PE meshes reached 60.91%, 70.62%, and 69.96%, the drag force coefficient of the mesh was the smallest (Figure 11d–f). This may be because, with the gradual increase in biological attachment, the surface of the mesh also becomes rough. When the organisms continue to increase, the newly attached organisms fill the gap between the former organisms and the mesh such that the gap between the attached organisms is closed. When the attachment density of organisms sequentially increases (>75% for PET and UHMWPE, >90% for PE), the attached organisms completely block the mesh, and the drag force coefficient of the mesh reaches a larger value. Bi et al. [17] found that the drag force coefficient of the mesh increased with the increase in the density of biological adhesion, possibly because the attached organisms were mainly hydroids. The abundance of attached organisms did not increase when they reached a certain level, and the gaps between them could not be filled. Thus, the surface roughness of the mesh remained unchanged. Therefore, the drag force coefficient of the mesh was positively correlated with the density of attached organisms. The experimental results showed that the attached organisms on the mesh were algae and crustaceans, and the gap created by the increase in crustaceans could be filled by algae. The surface of crustaceans is relatively smooth compared with that of hydroids. The drag force increased with the net solidity ratio and biological adhesion volume, with considerable dispersion, which is attributed to the different kinds of biofouling. Many fouling organisms are associated with cages, such as hydroids, mussels, and algae [21]. The physical and geometric characteristics of biological fouling and its various distribution forms have different effects on the hydrodynamic characteristics of the cage.

3.4. The Effect of Biological Adhesion on the Hydrodynamics of Nets Based on the BP Neural Network

BP neural network training was used to predict the influence of the characteristics of average thickness and average density on the drag force of the mesh, and the results are shown in Figure 12. For BP neural network training based only on flow velocity and

average thickness, fitting yielded an R^2 = 0.87. For the BP neural network training based only on flow velocity and average density, fitting yielded an R^2 = 0.90, suggesting that the BP neural network training based on flow velocity, average thickness, and average density showed a fitting with R^2 = 0.94. The results showed that compared with the average thickness, the density of biological adhesion had a greater effect on the drag force of the mesh.

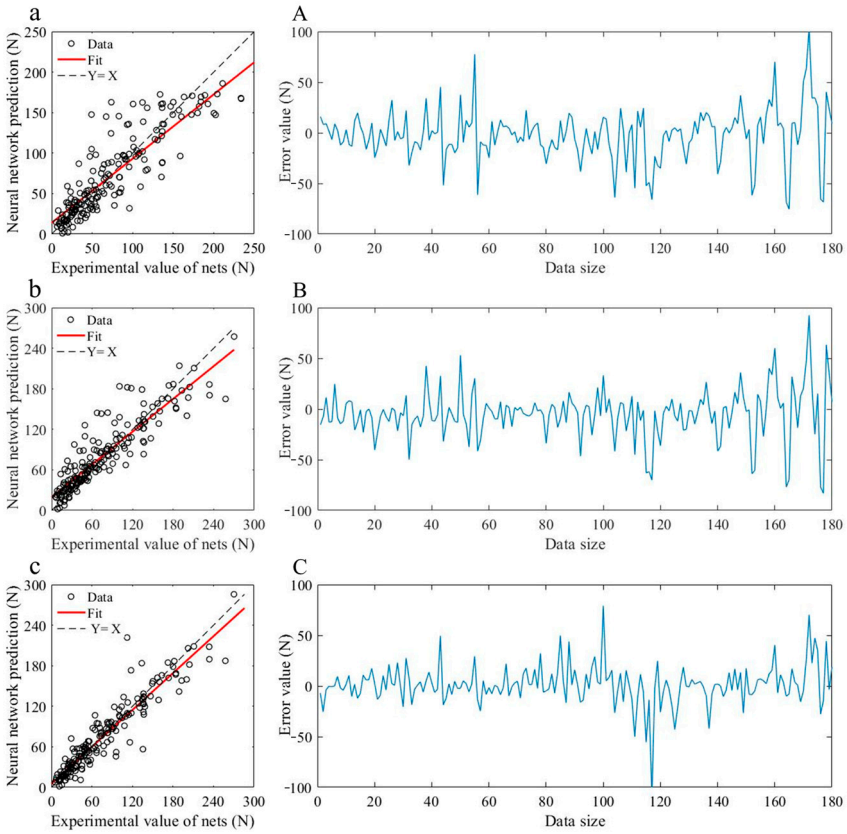

Figure 12. The relationship and the error value between the BP neural network predictions and the experimental values of the nets ((**a**,**A**): only biological adhesion thickness was used; (**b**,**B**): only biological adhesion density was used; (**c**,**C**): both biological adhesion thickness and density were used).

In general, the solidity ratio of the fluid-fouled net and the density and thickness of the biofouling are related to the drag force acting on the biofouled net. For the fluid passing through the biofouled net, the drag force is mainly from the pressure drop, largely dependent on the projected area. Therefore, the density of attached organisms has a greater influence on the drag coefficient than the thickness of biological fouling. Therefore, the training results of the BP neural network constructed using only the density of biological attachment were closer to the measured values. Based on this model, image analysis can be combined with photos of fluid-contaminated nets, and the drag coefficients of the nets under different materials, different months, and different fluid levels can be obtained. Once the drag coefficient of the fluid-contaminated net is obtained, existing predictions of the net drag force performance can be used [25,26]. The main advantage of this method is that some panel net components can be deployed around the cage, and by observing the biological adhesion characteristics of the panel net in different months, the hydrodynamic load of the full-size cage can be estimated.

The density of the mesh was processed based on the mesh photos in this study (5 flow velocities × 3 material nets × 12 months = 180 data). Since the attached organisms are flexible, their position and shape are prone to shifting and deformation, thus affecting the projected area of the biological attachment net. In the flume physics experiment, the attached organisms are streamlined under the impact of water flow. In this case, the

projected area of the organism's attachment changed with the flow velocity. However, it is difficult to quantify the state and projected area of the attached organism under the impact of the current. Therefore, in this study, the density of the biological pollution net refers to the proportion of the biological attachment area independent of the flow velocity in the total area of the net. The biological attachment thickness is the biological attachment thickness when the mesh is vertically placed. Therefore, future studies should quantify the effects of different types of biological pollution on the hydrodynamic characteristics of the net [15,16].

Based on the BP neural network training model fitting test data, it was found that the errors of the predicted and measured drag force of the PET, UHMWPE, and PE biological adhesion nets in different months and flow velocities were 3.9%, 1.5%, and 4.8%, respectively (Figure 13). This proves once again that BP neural network training can predict the drag force of biological adhesion nets based on the density and thickness of biological adhesion.

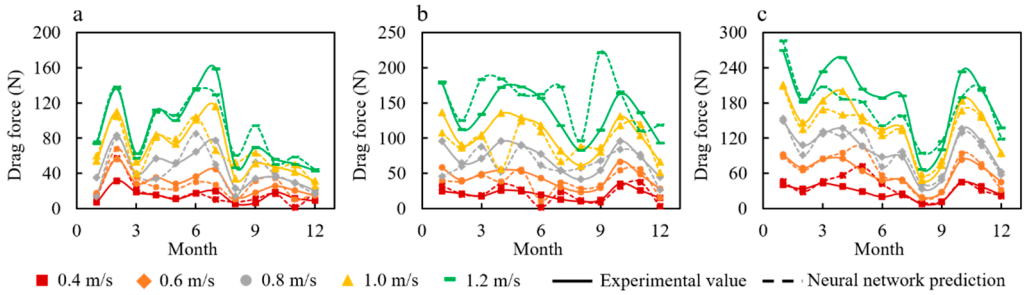

Figure 13. Comparison between the drag force predicted by the BP neural network and the actual experimental values ((**a**): PET; (**b**): UHMWPE; (**c**): PE).

Through the investigation, it was found that aquaculturists usually clean and maintain the cages regularly. The BP neural network training can effectively make fast and accurate predictions according to the test data. The current research involves establishing a cleaning and maintenance plan for the biologically attached nets according to the relationship between the density and thickness of biological adhesion and the drag force of the nets through training. By doing so, it can not only reduce unnecessary cleaning by aquaculturists and effectively ensure the water permeability of the cage, but also realize the automation of cage cleaning and maintenance, ultimately resulting in cost savings. In addition, corresponding cleaning and maintenance plans according to different materials of nets can also be made. For the PET mesh, the biological adhesion increases rapidly in spring and summer, resulting in a significant increase in net drag force. Therefore, the frequency of mesh cleaning can be increased. The amount of biological adhesion increases slowly in autumn and winter, and the frequency of washing can be appropriately reduced. Moreover, the annual biological adhesion of UHMWPE and PE meshes can cause the mesh to have high drag force, so the mesh can be set to be cleaned once a month or every two months. It is recommended to use a PET net as the main material of the cage to reduce the negative impact of biological adhesion on the net.

4. Conclusions

There are serious negative effects of biofouling in aquaculture cages. Quantifying the effects of biological pollution with various physical and geometric characteristics on the hydrodynamics of an aquaculture net is urgent. Through field sampling, we determined that the main biological fouling on the fishing nets in the Fujian area of the East China Sea was by crustaceans, mollusks, and algae, and the average thickness of the nets attached was 12.4–30.9 mm. The thickness and density of biological adhesion varied seasonally, being highest in the summer and lowest in the winter.

The difference in drag force of PET, UHMWPE, and PE nets and the characteristics of hydrodynamic performance under different biological adhesion conditions in different

months were investigated by physical experiments using a flume tank. In general, the drag force coefficient of clean PET mesh was the lowest (~0.53), and those of UHMWPE and PE meshes were 161.2% and 133.5% higher, respectively. With the increase in the biological pollution level, the drag force acting on the net also increased. Biological attachment in the PET mesh was the lowest, with the lowest relative drag force coefficient, indicating that the PET net has a good anti-fouling property. Based on BP neural network training, the relationship model between the biological adhesion characteristics (thickness and density) and the drag force characteristics of the net was established. The biological adhesion density had a stronger effect on the drag force performance of the mesh than the biological adhesion thickness. Additionally, the accuracy of predicting the drag force of nets only by the density and thickness still needs to be improved, and the shape of the biological attachment net when impacted by the current underwater is completely different from that on the laboratory measuring table, which affects the accuracy of the measured density and thickness data. Therefore, the measurement methods for the density and thickness of the net also need to be improved in future research.

Author Contributions: Methodology, Y.L., L.W. (Liang Wang) and S.M.; Software, W.L.; Validation, S.M.; Formal analysis, M.M.; Investigation, Y.L.; Resources, L.W. (Lei Wang) and M.M.; Data curation, W.L. and L.L.; Writing—original draft, Y.L.; Writing—review & editing, W.L. and L.W. (Liang Wang); Project administration, L.W. (Lei Wang); Funding acquisition, L.W. (Lei Wang). All authors have read and agreed to the published version of the manuscript.

Funding: This study was financially sponsored by the Central Public-interest Scientific Institution Basal Research Fund, CAFS (NO.2024XT08, NO.2024XT0802), the Basic research expenses of Chinese Academy of Fishery Sciences (2023TD82), the National Natural Science Foundation of China (32173026), the Marine S&T Fund of Shandong Province for Qingdao Marine Science and Technology Center (No. 20220NLM030001-4), and the Special Fund for Science and Technology Development in Zhanjiang City, Guangdong Province (2022A01037).

Institutional Review Board Statement: Not applicable.

Informed Consent Statement: Not applicable.

Data Availability Statement: Data is contained within the article.

Conflicts of Interest: The authors declare no conflict of interest.

References

1. Edwards, P.; Zhang, W.; Belton, B.; David, C.L. Misunderstandings, myths and mantras in aquaculture: Its contribution to world food supplies has been systematically over reported. *Mar. Policy* **2019**, *106*, 103547. [CrossRef]
2. Braithwaite, R.A.; Carrascosa, M.C.C.; McEvoy, L.A. Biofouling of salmon cage netting and the efficacy of a typical copper-based antifoulant. *Aquaculture* **2007**, *262*, 219–226. [CrossRef]
3. Phillippi, A.L.; O'Connor, N.J.; Lewis, A.F.; Kim, Y.K. Surface flocking as a possible anti-biofoulant. *Aquaculture* **2001**, *195*, 225–238. [CrossRef]
4. Eckman, J.E.; Thistle, D.; Burnett, W.C.; Paterson, G.L.J.; Roberston, C.Y.; Lambshead, P.J.D. Performance of cages as large animal-exclusion devices in the deep sea. *J. Mar. Res.* **2001**, *59*, 79–95. [CrossRef]
5. Cronin, E.R.; Cheshire, A.C.; Clarke, S.M.; Melville, A.J. An investigation into the composition, biomass and oxygen budget of the fouling community on a tuna aquaculture farm. *Biofouling* **1999**, *13*, 279–299. [CrossRef]
6. Tan, C.K.F.; Nowak, B.F.; Hodson, S. Biofouling as a reservoir of *Neoparamoeba pemaquidensis* (Page, 1970), the causative agent of amoebic gill disease in Atlantic salmon. *Aquaculture* **2002**, *210*, 49–58. [CrossRef]
7. Waddy, S.L.; Burridge, L.E.; Hamilton, M.N.; Mercer, S.M.; Aiken, D.E.; Haya, K. Emamectin benzoate induces molting in American lobster, *Homarus americanus*. *Can. J. Fish. Aquat. Sci.* **2002**, *59*, 1096–1099. [CrossRef]
8. Hodson, S.L.; Burke, C.M.; Bissett, A.P. Biofouling of fish-cage netting: The efficacy of a silicone coating and the effect of netting colour. *Aquaculture* **2000**, *184*, 277–290. [CrossRef]
9. Guo, Y.C.; Mohapatra, S.C.; Guedes Soares, C. Review of developments in porous membranes and net-type structures for breakwaters and fish cages. *Ocean Eng.* **2020**, *200*, 107027. [CrossRef]
10. Lader, P.; Fredriksson, D.W.; Guenther, J.; Volent, Z.; Blocher, N.; Kristiansen, D.; Gansel, L. Drag on hydroid-fouled nets—An experimental approach. *China Ocean Eng.* **2015**, *29*, 369–389. [CrossRef]
11. Farshad, N.K.; Mostafa, Z.; Taghi, A.; Mehdi, B. Wave attenuation/build-up around and inside marine fouled floating aquaculture cages under regular wave regimes. *J. Ocean Eng. Mar. Energy* **2021**, *7*, 59–81. [CrossRef]

12. Bi, C.W.; Zhao, Y.P.; Dong, G.H.; Cui, Y.; Gui, F.K. Experimental and numerical investigation on the damping effect of net cages in waves. *J. Fluids Struct.* **2015**, *55*, 122–138. [CrossRef]
13. Bi, C.W.; Xu, T.J. Numerical study on the flow field around a fish farm in tidal current. *Turk. J. Fish. Aquat. Sci.* **2018**, *18*, 705–716. [CrossRef] [PubMed]
14. Bi, C.W.; Zhao, Y.P.; Dong, G.H.; Xu, T.J.; Gui, F.K. Numerical study on wave attenuation inside and around a square array of biofouled net cages. *Aquacult. Eng.* **2017**, *78*, 180–189. [CrossRef]
15. Swift, M.R.; Fredriksson, D.W.; Unrein, A.; Fullerton, B.; Patursson, O.; Baldwin, K. Drag force acting on biofouled net panels. *Aquacult. Eng.* **2006**, *35*, 292–299. [CrossRef]
16. Gansel, L.C.; Plew, D.R.; Endresen, P.C.; Olsen, A.I.; Misimi, E.; Guenther, J.; Jensen, Ø. Drag of clean and fouled net panels-measurements and parameterization of fouling. *PLoS ONE* **2015**, *10*, 0131051. [CrossRef]
17. Bi, C.W.; Zhao, Y.P.; Dong, G.H.; Wu, Z.M.; Zhang, Y.; Xu, T.J. Drag on and flow through the hydroid-fouled nets in currents. *Ocean Eng.* **2018**, *161*, 195–204. [CrossRef]
18. Dos Santos, A.P.; Hage Seta, J.H.; Kuhnen, V.V.; Sanches, E.G. Antifouling alternatives for aquaculture in tropical waters of the Atlantic Ocean. *Aquacult. Rep.* **2020**, *18*, 100477. [CrossRef]
19. Bi, C.W.; Chen, Q.P.; Zhao, Y.P.; Su, H.; Wang, X.Y. Experimental investigation on the hydrodynamic performance of plane nets fouled by hydroids in waves. *Ocean Eng.* **2020**, *213*, 107839. [CrossRef]
20. Dong, S.; You, X.; Hu, F. Effects of design factors on drag forces and deformations on marine aquaculture cages: A parametric study based on numerical simulations. *J. Mar. Sci. Eng.* **2020**, *8*, 125. [CrossRef]
21. Bloecher, N.; Olsen, Y.; Guenther, J. Variability of biofouling communities on fish cage nets: A 1-year field study at a Norwegian salmon farm. *Aquaculture* **2013**, *416*, 302–309. [CrossRef]
22. Guenther, J.; Misimi, E.; Sunde, L.M. The development of biofouling, particularly the hydroid Ectopleura larynx, on commercial salmon cage nets in Mid-Norway. *Aquaculture* **2010**, *300*, 120–127. [CrossRef]
23. Balash, C.; Colbourne, B.; Bose, N.; Raman-Nair, W. Aquaculture net drag force and added mass. *Aquacult. Eng.* **2009**, *41*, 14–21. [CrossRef]
24. Patursson, Ø.; Swift, M.R.; Tsukrov, I.; Simonsen, K.; Baldwin, K.; Fredriksson, D.W.; Celikkol, B. Development of a porous media model with application to flow through and around a net panel. *Ocean Eng.* **2010**, *37*, 314–324. [CrossRef]
25. Bi, C.W.; Zhao, Y.P.; Dong, G.H.; Xu, T.J.; Gui, F.K. Numerical simulation of the interaction between flow and flexible nets. *J. Fluids Struct.* **2014**, *45*, 180–201. [CrossRef]
26. Chen, H.; Christensen, E.D. Development of a numerical model for fluid-structure interaction analysis of flow through and around an aquaculture net cage. *Ocean Eng.* **2017**, *142*, 597–615. [CrossRef]